Chapter 8

Detector Solenoid and Iron Structure

8.1 Solenoid Magnet

The solenoidal magnet provides an axial magnetic field of about 1.5 Tesla over the tracking volume of BELLE. The magnetic field produced by the coil is returned by the steel plates of the surrounding K_L-catcher and muon detector. The overall characteristics of the magnet are summarized in Table 8.1.

Table 8.1: Magnet Characteristics

Cryostat	Inner Radius	min 1.7 m
	Outer Radius	max 2.0 m
	Total Length	max 4.44 m
Nominal Magnetic Field		1.5 T
Cool Down Time		$\leq$ 6 days
Quench Recovery Time		$\leq$ 1 day

8.1.1 Magnetic Field Design

The field uniformity and forces on the coil are strongly influenced by the proximity of the iron elements of the K_L-catcher, the effects of which are calculated in a series of axially symmetric finite-element models using the ANSYS program. The field uniformity in the tracking volume is discussed below in the context of the yoke structure.

Table 8.2: Decentering forces on the coil.

Axial decentering force	1.6×10^6 N/5cm
Radial decentering force	$< 2.6 \times 10^4$ N/cm

The axial and radial decentering forces are determined by perturbing the axial and radial coil positions relative to the endwall of the iron yoke structure which is nominally located 330 mm from the end of the current-carry section of the coil. The decentering forces are summarized in Table 8.2.

8.1.2 Coil Design

General Design

The magnetic field requirements can be realized using designs that has been used successfully for other solenoidal magnets. In particular, the configuration selected for the BELLE coil is similar to that of the TOPAZ solenoid, and consists of a single-layer aluminum-stabilized superconductor coil wound around the inner surface of an aluminum support cylinder. Indirect cooling is provided by liquid helium circulating through a single tube welded on the outer surface of the support cylinder.

Since the coil/cryostat thickness is not a concern for BELLE, the outer vacuum cylinder will be fairly thick, for example a 15 mm-thick stainless-steel plate.

Coil Parameters

The solenoid coil is shown in Fig. 8.1 . The coil windings are glued on the the inner surface of the aluminum (A5083) support cylinder. The coil parameters are summarized in Table 8.3.

Even if the total magnetic energy were dumped entirely into the conductor, the material of the 33 mm-thick coil would be sufficient to keep the coil temperature below 80 K after a quench at the 4000 A operating current. The primary issue regarding conductor fabrication is the cross sectional aspect ratio of the conductor. The conductor we use has a thickness of 3 mm with 2×0.1 mm turn-to-turn insulation. The electric ground insulation between the coil and the support cylinder must have breakdown voltage larger than 2kV.

The solenoid is required to be reliable against two main mechanical stresses:

- hoop and axial stresses inside the superconductor; and

Table 8.3: Parameters of the Solenoid Coil

Dimensions;		
Cryostat	Inner radius	1.70 m
	Outer radius	2.00 m
	Length	4.44 m
Coil	Effective radius	1.8 m
	Length	3.8 m
Conductor	Dimension	$3 \times 33\ mm^2$
Outer cylinder Thickness		15 mm
Electrical parameters;		
Center field		1.5 T
Nominal Current		4000 A
Inductance		4.3 H
Stored energy		35 MJ
Stored energy/cold mass (E/M)		6.5 kJ/kg
Typical charging time		0.5 hour
Mechanical parameter;		
Effective cold mass		$< 7ton$

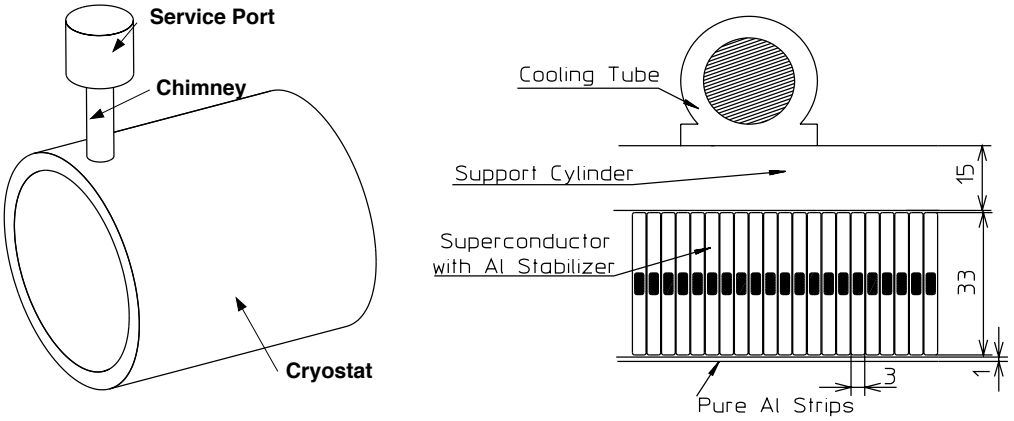

(a) Outlook of the magnet (b) Cross sectional view of the coil

Figure 8.1: The configuration of the superconducting coil.

- shear stresses at the boundary between the coil and the outer support cylinder caused by the axial electromagnetic force. These are maximum at the coil end.

The magnetic pressure P_r in a long solenoid is approximately

$$P_r = \frac{B_z^2}{2\mu_0} = 0.9\, MPa. \tag{8.1}$$

This produces a hoop stress, s_ϕ, in the coil and support cylinder given by

$$\begin{aligned} s_\phi &= \frac{R}{t} \times P_r \\ &= 35\, MPa, \end{aligned} \tag{8.2}$$

where R is the coil radius and t is the total coil plus outer cylinder thickness. The axial compressive force in a long solenoid is approximately

$$\begin{aligned} F_z &= \frac{dE}{dz} \\ &\simeq \frac{d}{dz}\left(\frac{B_z^2}{2\mu_0} Sz\right) \\ &\simeq \frac{B_z^2}{2\mu_0} S \\ &= 9.1\, MN, \end{aligned} \tag{8.3}$$

where E is the stored energy, z is the dimension along the coil axis, and S is the area of the effective magnetic aperture. The axial magnetic force in the present design is reduced to $F_z = 6.4MN$, because the attractive force works between the end yoke and the coil. Therefore, the resultant axial stress becomes approximately

$$\begin{aligned} s_z &= \frac{F_z'}{2\pi Rt} \\ &= -12MPa, \end{aligned} \tag{8.4}$$

where the negative sign indicates a compressive stress. These two stresses accumulate at the coil center where the maximum combined stress is given by

$$\begin{aligned} 2\tau &\simeq (s_\phi - s_z) \\ &= 47\,MPa\ (< \sigma_y = 67\,MPa). \end{aligned} \tag{8.5}$$

The shear stress at the epoxy bond between the coil and support cylinder is another important mechanical parameter. A rough estimate for the maximum value for this shear stress in the most pessimistic case is

$$\begin{aligned} F_z &= B_r \times I \\ &= 6000 N/m, \end{aligned} \tag{8.6}$$

at the end of coil. We assume that this axial force is supported by radial outer surface of the coil, giving a shear at the outer boundary of (approximately)

$$\begin{aligned} s_{shear} &= \frac{F_z}{W_z} \\ &< 2\,MPa, \end{aligned} \tag{8.7}$$

where W_z is the axial width of the conductor. This number is at least four times smaller than the shear stress measured in various sample tests for the SDC detector magnet. The actual shear stress will be also smaller than those estimated by this simple model calculation. A finite element analysis has been carried out to obtain a more precise estimate of this stress. Figure 8.2 shows the FEA results for the forces on the coil and the resulting deformation. This figure demonstrates that the strain would be less than 0.1.

In order to satisfy the design requirement of a maximum temperature of less than 80 K after a quench without a dump resistor, the stored energy must be dumped as uniformly as possible into the coil. This is possible if the quench propagation time constant is much faster than the time constant of the power dissipation during the quench. A technique to increase the propagation velocity of the quench via pure aluminum strip quench propagators has been verified experimentally in the construction of a thin superconducting solenoid for a balloon experiment.[1] In the present design, 2-mm thick, pure aluminum strips are wound on the inner surface of the coil. Figure 8.3 shows the estimated temperature increase after a quench with a 0.1Ω dump resistor. This demonstrates that the coil absorbs entire stored energy safely.

8.1.3 Superconductor design

In the VENUS and TOPAZ solenoids, superconducting wire stabilized with 99.999%-purity aluminum (RRR $>$ 1000) was used. However, recent R&D for the SSC magnet

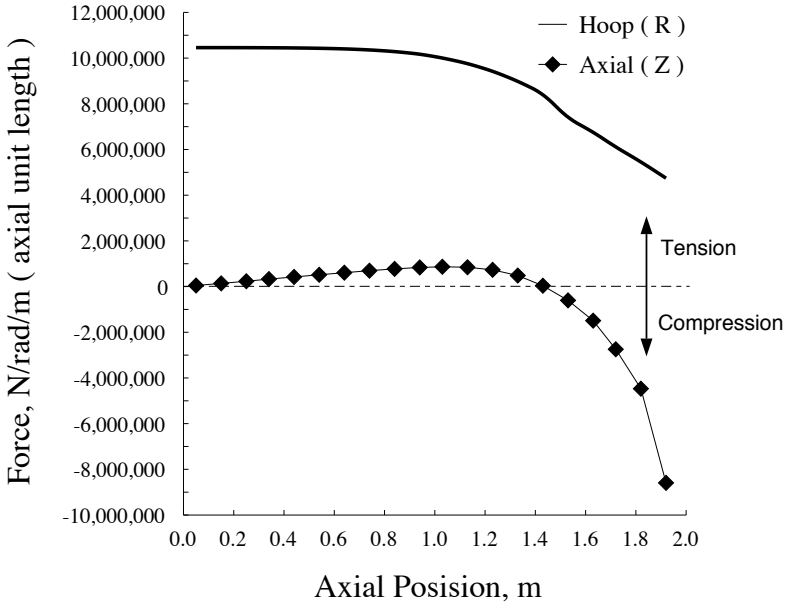

Figure 8.2: Radial and axial components of the force on the coil.

has demonstrated that aluminum with a purity of 99.99 % would be sufficient if the stabilizer has a sufficient cross section. This type of conductor, which is less expensive than the five-nine purity aluminum, was used for the CLEO-II and the ALEPH magnets with no technological problems.

The superconducting cable is co-extruded with aluminum so that the superconducting cable is at the center of the aluminum stabilizer. Figure 8.4 shows the superconductor and magnet characteristics of the cable. The 4000 A operating point will be 50% along the load line of the conductor. The stability of the superconductor against a quench is one of the most important issues in the conductor design. It is parameterized by the minimum quench energy (MQE). For the present conductor design, the MQE is expected to be 1.3 J.

8.1.4 Cryostat

Radiation Shield

Radiation shields made of aluminum alloy foils are placed between the coil and the vacuum vessel walls. The shields are connected to the end flanges to become a single coaxial unit supported from the vacuum vessel. This shield is, however, decoupled electrically from both the coil and the vessel walls in order to avoid the effects of the eddy current induced by the fast current discharge of the coil. The cooling paths have similar radiation shields.

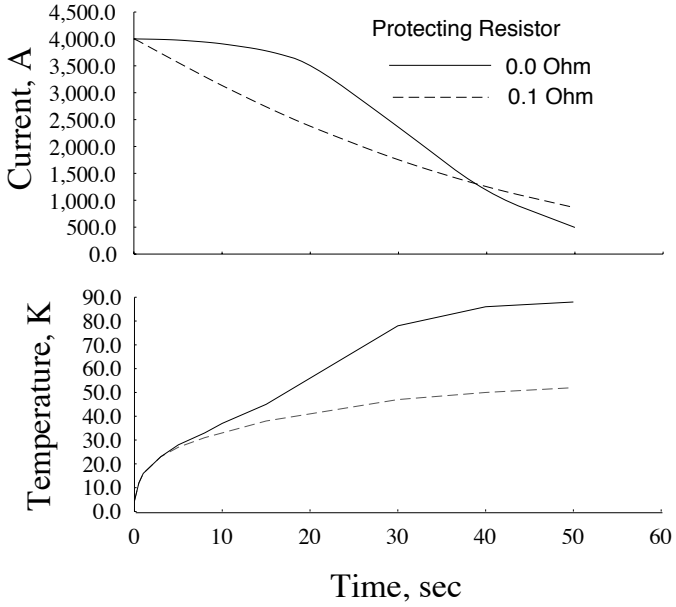

Figure 8.3: Quench behavior of the coil with pure aluminum strips.

Cryostat Vacuum Vessel

The vacuum vessel for this magnet consists of inner and outer coaxial cylinders that are connected by flat annular bulkheads at each end. The coil is suspended inside the vacuum vessel by the support system described below. The superconducting leads and cryogenic pipes go though a chimney penetration in the wall of the vacuum vessel. The vacuum vessel is made of a non-magnetic metal.

Coil Support

The purpose of the support system is to transmit both the weight of the cold mass and the electromagnetic decentering forces to the outer iron structure. The cold mass of the outer support cylinder, conductor, and insulator is approximately 7 tons. The magnetic force (F_Z) of 160 tonF is larger than the gravitational force and, thus, dominates the deisgn of support structure.

If the iron structure is symmetric around the electromagnetic center of the coil and the coil is located with no declination, the coil would be in unstable equilibrium with no net electromagnetic forces acting upon it. However, if the coil were displaced from this position, forces would act on the coil in such a way to increase the displacement. The support system is designed to sustain forces from a maximum displacement of 20 mm from the equilibrium position. If the iron structure is not symmetric, such as in the case of the DIRC PID option, the magnet center has to be adjusted by changes in the coil wind-spacing.

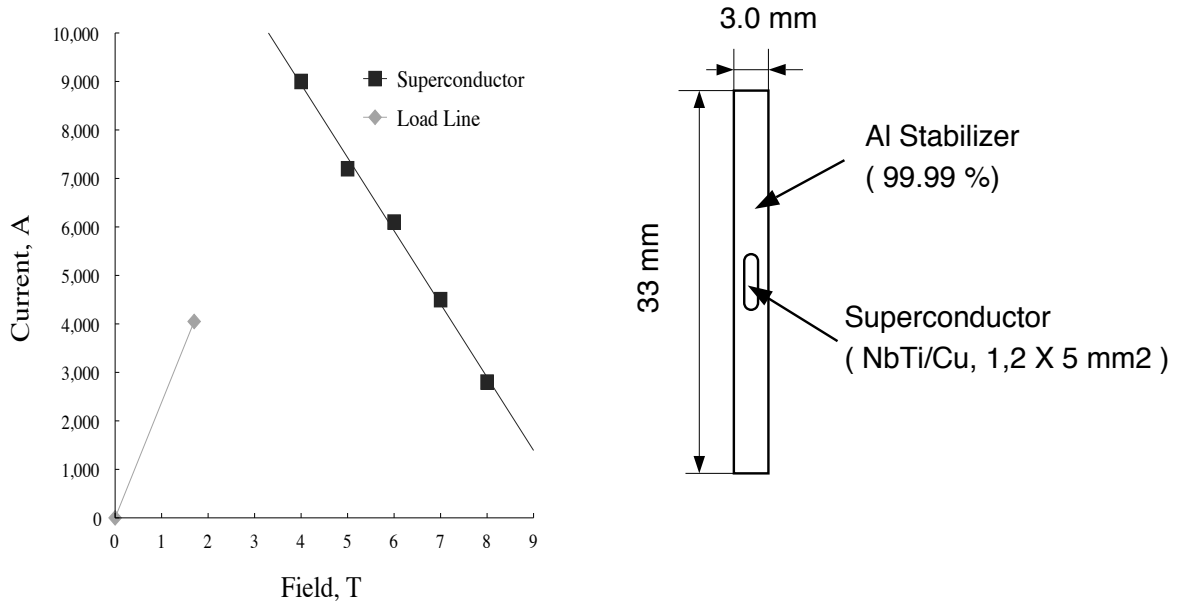

Figure 8.4: Configuration of superconductor and its characteristics in the magnet.

Chimney

The cryogenic lines and the superconducting leads from the coil go through the chimney to the service port outside of the iron structure. The lines and leads are surrounded by multi-layer thermal shields and the vacuum jacket. A part of the vacuum jacket has a sliding sleeve for the access to the tubing joints in the cryogenic lines, the superconducting leads, and the thermal shields. It has also a connector box to house hermetic high voltage and instrumentation connectors. The chimney protrudes vertically upward from one end of the coil. The annular space between the thermal shield and the vacuum jacket is occupied by the flow channels for the pressure relief and vacuum exhaust lines. Pressure relief is needed to protect the vacuum vessel from overpressure in the event of an accidental leak of cryogens from the cooling line. The relief device and vacuum pump are located on the service port. A hole of dimension 50×50 cm^2 in the iron yoke accommodates the chimney.

Because of the size limitation, the chimney, the superconducting leads, the cryogen lines, and the service port are disconnected from the coil during transport and connected at the Tsukuba hall. The tubing joints in the cryogenic lines are configured in the chimney in such a way as to provide easy access during installation.

The connectors for coil monitoring devices are located on the chimney, close to the cryostat, and are accessible from the front end surface of the barrel yoke.

Thermal Design and Cool Down Characteristics

The coil is cooled by the forced flow of two phase helium similar to the method used for the CDF and TOPAZ coils. The axial and radial distance between the coil and the thermal shield is designed so that they do not touch during the pre-cooling induced thermal contractions. We estimate the heat load at the normal operation would be 20 W including a 20% margin.

8.1.5 Cryogenics

The baseline for the cryogenic system is the use of the existing TOPAZ refrigerator suitably modified for BELLE as shown in Fig. 8.5.

However, the TOPAZ refrigeration system has been operated for 43,000 hours and requires considerable effort to maintain. Many of the components of this system must be overhauled for the BELLE experiment. The experts who will operate this system for BELLE have proposed a new system with a simpler operational concept. The proposed system would not require around-the-clock operators as is the case for the current TOPAZ cryogenic system, and would eliminate the need for annual shutdowns for inspection. The extra cost of building the new system would be recovered in four years from reduced operating costs.

8.1.6 Power Supply

The power source currently used for the TOPAZ magnet will be converted for this magnet. It has a capacity of 5000 A and 15 V. The dump resistor needs to be modified. Figure 8.6 describes the protection circuitry for the magnet coil.

Three modes of switching and discharging are available for the extraction of the electromagnetic stored energy from the magnet. A fast discharge system will quickly switch off the circuit and extract the energy to the dump resistor. This mechanism must work during power failures and, therefore, the switch should be a power-to-close type and the dump resistor should be an adiabatic type that can be cooled by the natural air convection only. It is required to have sufficient redundancy in the fast discharge system and quench detectors for safe quench protection. A slow discharge system will discharge the coil sufficiently slowly so that the eddy current in the coil will not initiate a quench. This will be done by slowly running down the current set point.

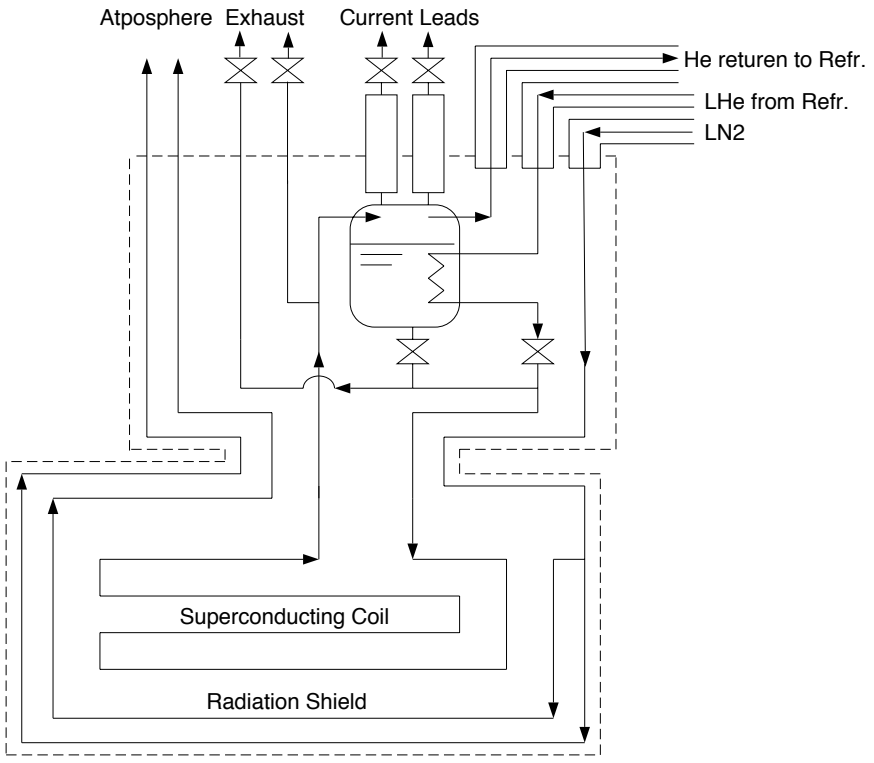

Figure 8.5: A proposed cryogenics system.

8.2 Iron Structure

8.2.1 General design

The structure consists of the barrel- and two end-yoke sections indicated in Fig. 8.7, which shows the baseline configuration of the BELLE structure.
The overall height is about 9 meters; the depth is about 8 meters. The structure will be made from low-carbon steel, have a total weight of approximately 1400 tonnes, and will be placed on the modified TOPAZ stand. The magnet center is 470 mm to the backward-angle side of the interaction point. An 80 mm air gap between the barrel and end yokes will be reserved for cable penetrations. During the roll-in and roll-out operations, the detector will be moved by the hydraulic jack system that is already in-place on the TOPAZ stand. The end-yoke separates at its center and then opens. The weight of each section is listed in Table 8.4. The total inner detector weight is approximately 80 tonnes.

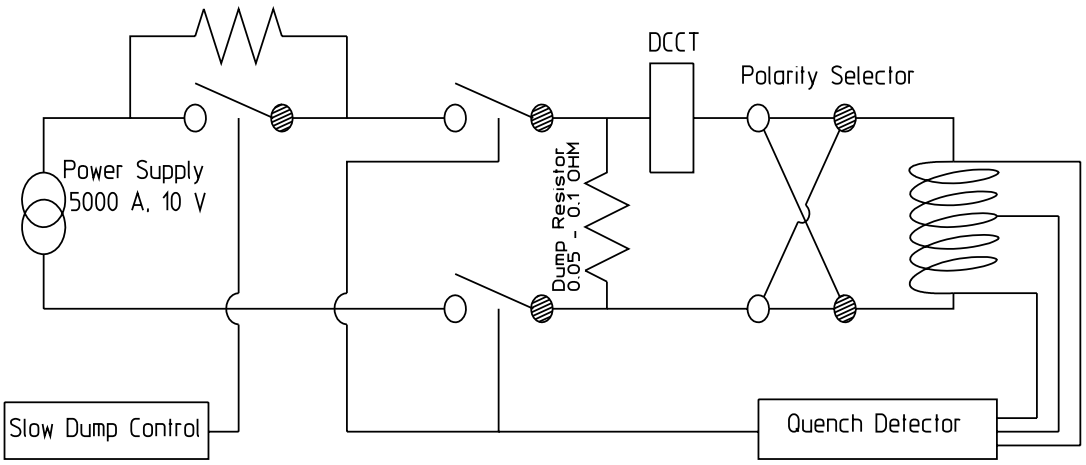

Figure 8.6: Protecting circuit in the Magnet Power Supply.

8.2.2 Barrel Yoke Structure

The barrel-yoke structure, shown in a isometric view in Fig. 8.8, is constructed from eight flux-return sections and eight K_L/μ detector modules. Each barrel K_L/μ module consists of 14 layers of 50 mm-thick steel plates interspersed with 15, 40 mm-thick instrumented gaps. The iron plates of the K_L/μ catcher are required to within ± 2 mm of being flat. Outside this is the 200 mm thick flux-return section. Two types of supports will be mounted on the strucutre: one, a centipede-like element, is used to fix each segment during the structure assembly procedure; the other, mounted after K_L/μ assembly is complete, will provide rigidity to the completed structure. The configuration of these supports is shown in Fig. 8.9.

A 500×500 mm^2 vertical slot located at the backward-angle side accomodates the chimney of the BELLE solenoid. The size of this slot will likely change as the solenoid design progresses.

This 600-tonne barrel-yoke structure must have a natural frequency higher than 5 Hz in order to avoid earthquake-driven resonances. The criteria against tare-deformation is ± 2 mm. The maximum tare deformation is estimated to be 1.5 mm. A complete structural analysis to determine the maximum deformation, the stress concentration on each support, and the natural freqency still has to be done.

8.2.3 End yoke

Each end-yoke structure consists of K_L/μ detector modules, 200 mm-thick flux-return sections and the pole tip. The K_L/μ modules have the same layer structure as those in the barrel. The coverage goes down to $\theta = 25^\circ$ as shown in Fig. 8.10.

The end yoke must withstand the 1000 tonne magnetic force from the detector

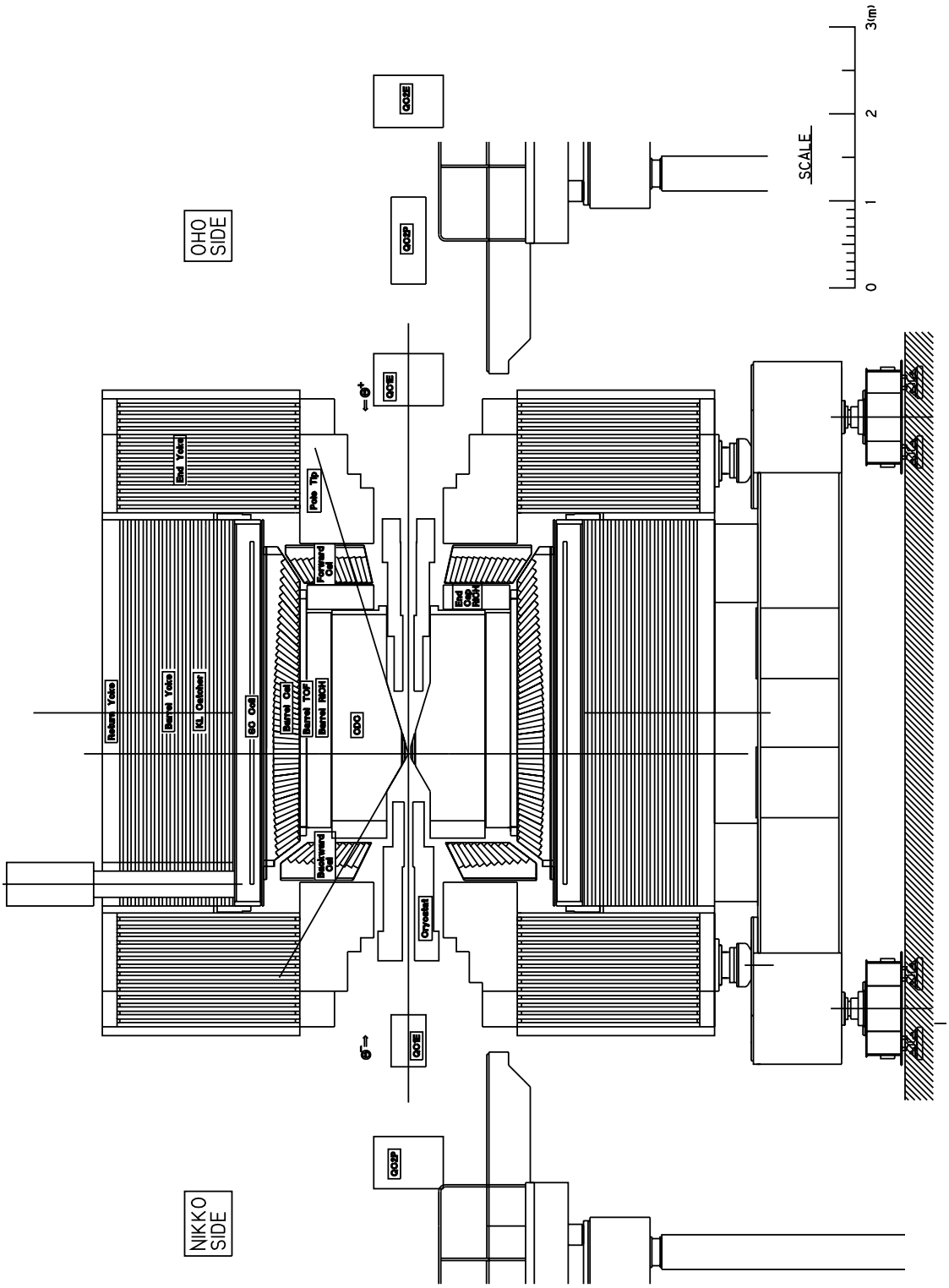

Figure 8.7: Side view of the BELLE detector.

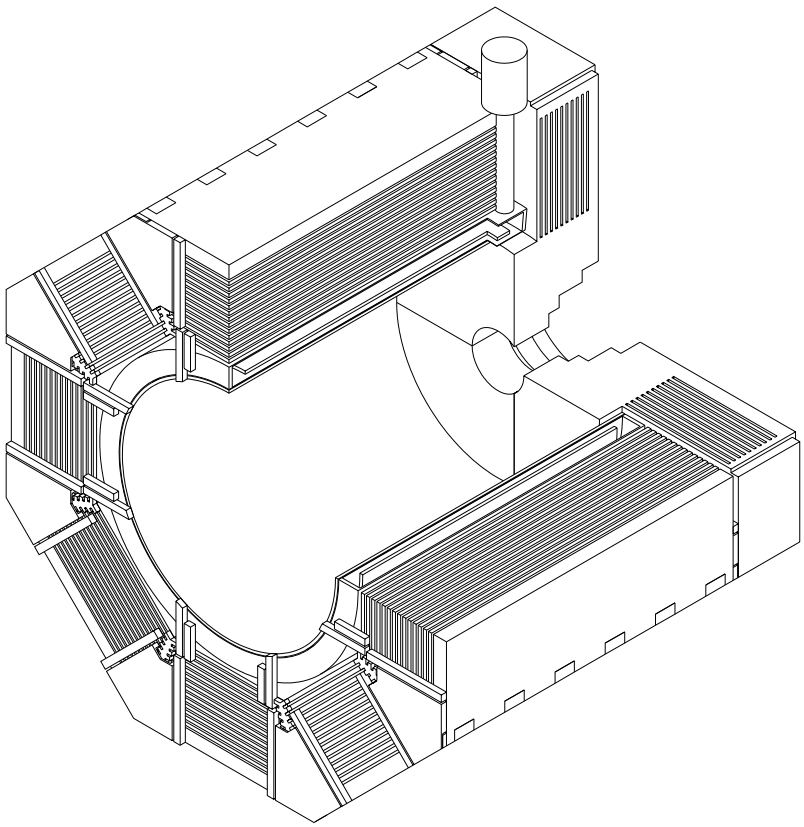

Figure 8.8: An isometric view of barrel yoke.

Table 8.4: The weight each part of the structure.

Barrel yoke part	Wt. of segment	Number of segments	Total weight
Flux-Return	19.5 tonnes	8	156 tonnes
K_L/μ-Module	55 tonnes	8	440 tonnes
Others			10 tonnes
Subtotal			606 tonnes
End yoke part	Wt. of segment	Number of segments	Total weight
Flux-Return	26 tonnes	4+4	208 tonnes
K_L/μ-Module	43.3 tonnes	4+4	346 tonnes
Pole tip	48 tonnes	1+1	96 tonnes
Subtotal			650 tonnes
Others			
TOPAZ stand			60 tonnes
Inner detector			80 tonnes
Total			1396 tonnes

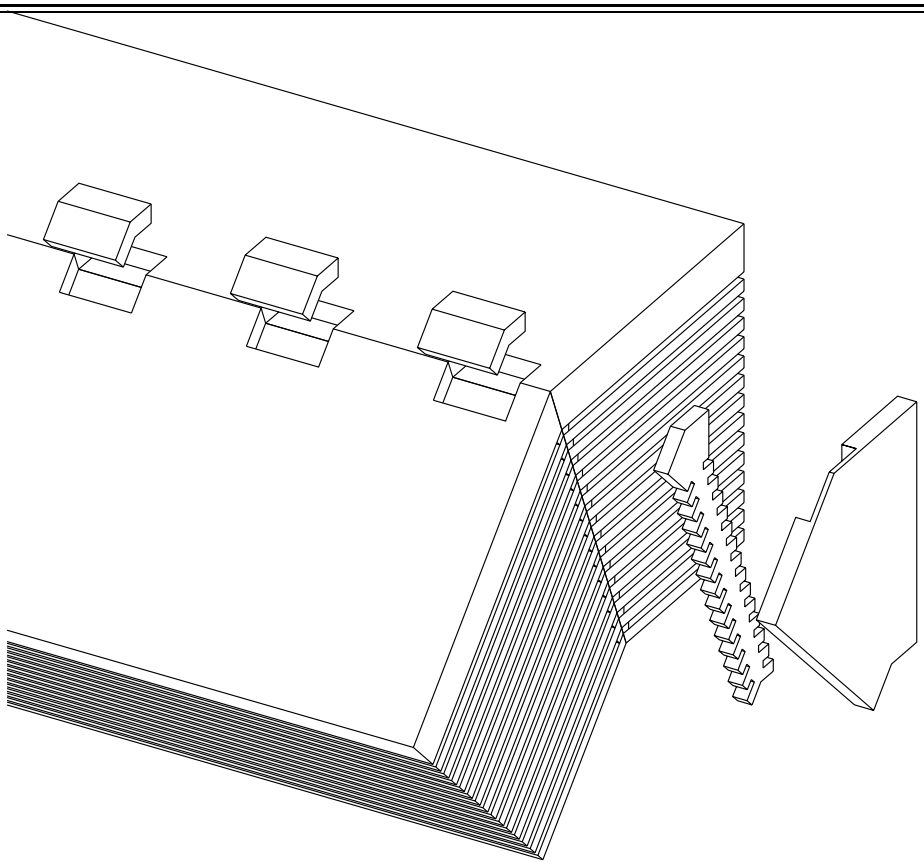

Figure 8.9: An isometric view of the support configuration.

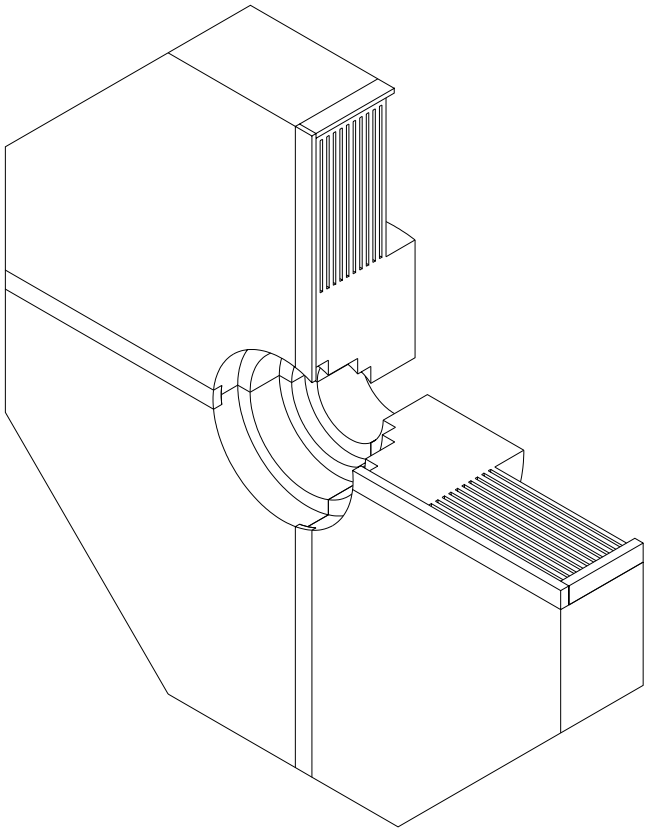

Figure 8.10: An isometric view of an end yoke.

solenoid. Each end-yoke is planned to separate into eight segments: four quadrents containing ten K_L/μ-catcher layers and four quadrents containing four K_L/μ-catcher layers and the flux return iron. This is done to keep each segment within the capacity of the 60 tonne crane. During assembly, the ten K_L/μ-catcher-layer sections will be built first followed by the four layer sections.

A finite-element-method calculation indicates a 0.8 mm deformation of the end yoke. In this calculation, the end yoke was taken to be a welded structure and only the ten layer K_L/μ-catcher was considered since the outer four-layer section is fixed in place by bolts. A 50 mm-thick of rib is located every 90 degrees in this calculation to help withstand the magnetic force.

Access to the Inner Detectors

The end-yoke must slide out to provide access to the inner detector. This motion will be strongly constrained both by the details of the end-yoke configuration and the support system for the KEKB IR magnets.

For the Aerogel and RICH PID options, access to the inner detector (i.e. the SVD, CDC and PID), will be made by horizontally moving the iron endcap. The endcap calorimeter and PID will be retracted on rails mounted to the endcap iron yoke. This procedure will be done without moving any accelerator components. An end-yoke transport system is being studied by several companies and various possibilities are being investigated. A conceptual design of one possibility is shown in Fig. 8.11.

For the DIRC option, the access to the CDC will be quite different. In this case, the endcap through which the quartz bars penetrate cannot be opened horizontally. We need to devise a proper supporting mechanism and endcap iron structure detectors over a span of about 4 m without touching the accelerator components. We do not have the engineering design for this option yet. We will work out this design in the coming few months so that we will be ready to request quotes in JFY95 no matter what PID option is chosen.

The structure assembly will be done in the rolled-out position. For the barrel yoke, the eight K_L/μ-catcher and return yoke segments will be assembled in the Tsukuba Hall pit after the modifications of the existing TOPAZ stand are complete. Temporary support fixtures may be required during assembly to prevent undue deformation. Similar considerations apply to the assembly of the end yokes.

Cable Penetrations

Cables will be extracted from the inner detector via an 80 mm air gap between the barrel and end yokes and in the space between the poletips and QCS. Figure 8.2.3 shows

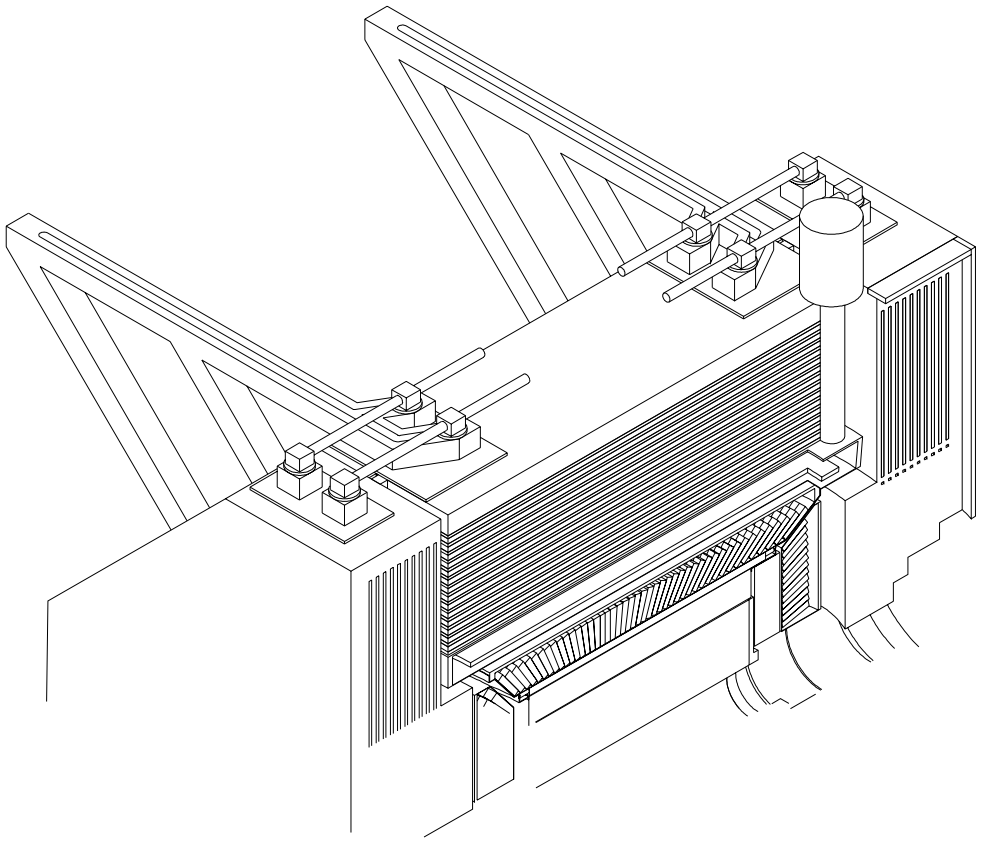

Figure 8.11: An isometric view of a possible end-yoke transport system.

the flow of cables from subdetectors. The number of cables from each subdetector are summarized in Table 8.2.3.

Table 2. Cables of Belle detector

8.3 Detector Supports

The plan for supporting each detector is not complete. The basic ideas are as follows:

- The detector solenoid is supported by a bar mounted on the end face of barrel yoke.
- The barrel CsI calorimeter is supported by stainless steel rings fixed to a support bar mounted the next to the solenoid support bar.
- The TOF system is mounted to the inner wall of the calorimeter.
- The PID device is supported by a cylinder attached to the barrel barrel calorimeter.
- The CDC is supported from the bottom of the PID end plate.
- The SVD and beam pipe are supported from the inner CDC wall.

8.4 Magnetic Field Calculation

The yoke configuration must be consistent with the requirements of a central axial field of 1.5 T provided by a coil with a 1.8 m free inner radius and a 1.97 m half length. The field uniformity in the CDC volume and field distribution along the beam axis were evaluated with a calculation that did not consider the influence of magnetic fields from the KEKB QC magnets. The calculated magnetic field distribution and flux line map are shown in Fig. 8.13.

The magnetic field in the pole tip exceeds 2.0 T driving the iron into saturation. The field value in the CDC volume is calculated to vary by 2.0%. The magnetic field along the beam line is shown in Fig. 8.14.

Table 8.5: Estimates of cables and other utilities coming out of the detector

detector	sgl/PC/gas	♯ of cables	type	x section	length
Barrel KL/MU	sgl	1440	t. pair	1.2cm^2	30m
	HV	1200	RG59	10mmϕ	30m
	gas	480	SUS	10mmϕ	30m
Endcap KL/MU	sgl	672	t. pair	15mmϕ	30m
	HV	224	RG59	30mmϕ	30m
	gas	224	SUS	1/2"^{2}	30m
Barrel Cal'meter	sgl	6624	t. pair	7mmϕ	10m
	liq/air clg	144/72	Cu	15mmϕ	10m
For'd Cal'meter	sgl	1168	t. pair	7mmϕ	10m
	liq/air clg	32/16	Cu	15mmϕ	10m
Back'd Cal'meter	sgl	1040	t. pair	7mmϕ	10m
	liq/air clg	32/16	Cu	15mmϕ	10m
Barrel TOF/TSC	sgl	512	1.5DQEV	3mmϕ	2m
	HV	184	Kurabe	3mmϕ	5m
	air clg	16	Cu	10mmϕ	30m
Barrel PID					
RICH option	sgl/stb/clk	60/60/60	t. pair	15mmϕ	10m
	PC	180	t. pair	10mmϕ	5m
	HV	120	RG174U	2.5mmϕ	5m
	gas/liq.rad	60/20	Cu/SUS	1/4"ϕ	5m
	air clg	10	Cu	1/2"ϕ	5m
Aerogel option	sgl	1920	RG174U	2.5mmϕ	5m
	HV	1920	RG174U	2.5mmϕ	5m
	air clg	6	Cu pipe	1/2"ϕ	5m
DIRC option	sgl	15,000	co-ax	5mmϕ	30m
	HV	15,000	co-ax	5mmϕ	30m
Endcap PID					
RICH option	sgl/stb/clk	24/24/24	t. pair	15mmϕ	10m
	PC	72	t. pair	10mmϕ	10m
	HV	48	RG174U	2.5mmϕ	10m
	gas/liq.rad	30/60	Cu/SUS	1/4"ϕ	10m
	air clg	10	Cu pipe	3/4"ϕ	10m
Aerogel option	sgl	268	RG174U	2.5mmϕ	10m
	HV	268	RG174U	2.5mmϕ	10m
CDC	sgl	524	t. pair	15mmϕ	30m
	HV	8-19 55	RG59B/U	10mmϕ	10+30m
	monitor	20	t. pair	3mmϕ	10m
	gas	10	SUS	1/4"ϕ	10+30m
SVD	scanner	432	Opt. fbr	2x7mm	30m
	PC	96	t. pair	6mmϕ	30m

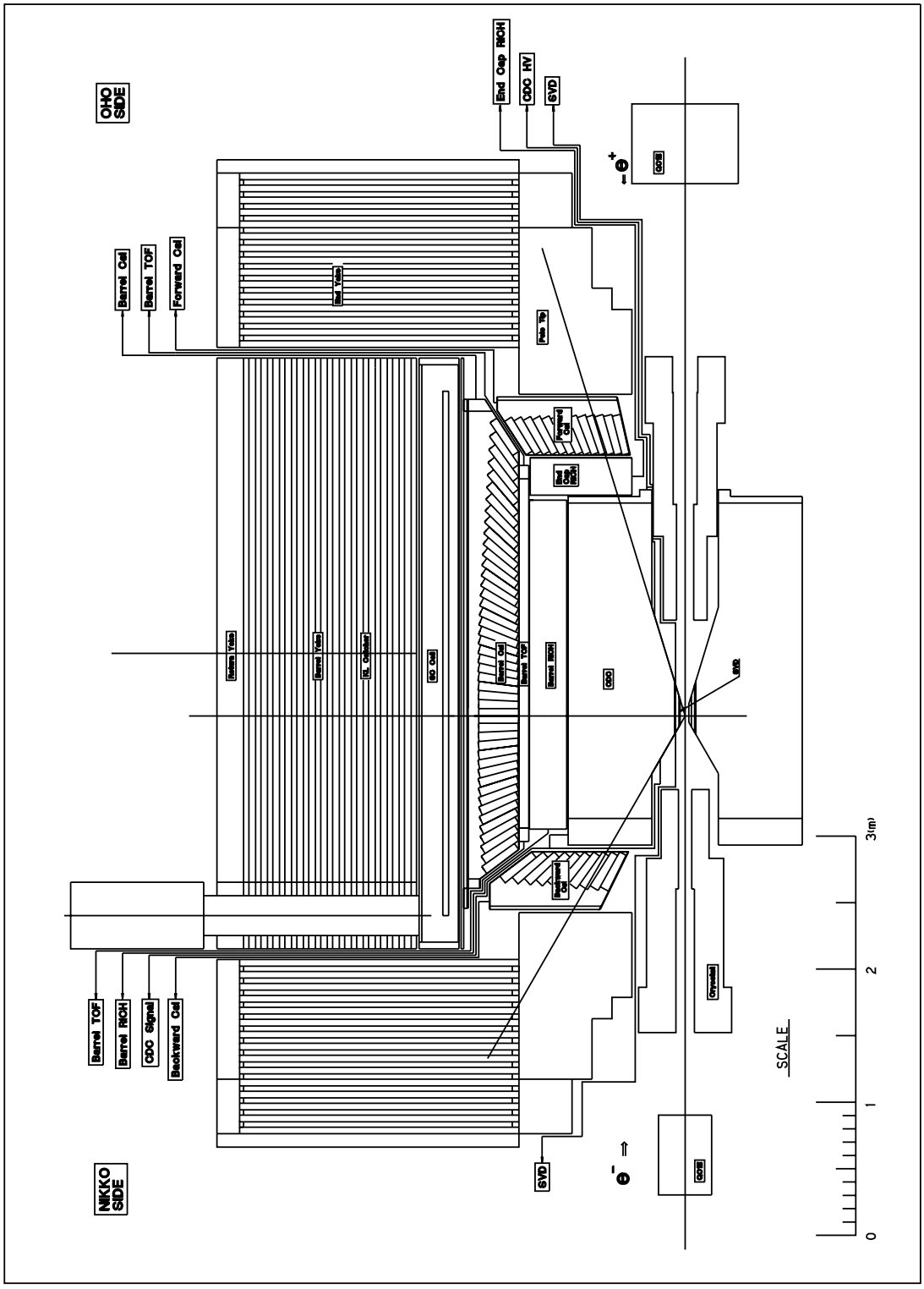

Figure 8.12: Flow of cables from subdetectors.

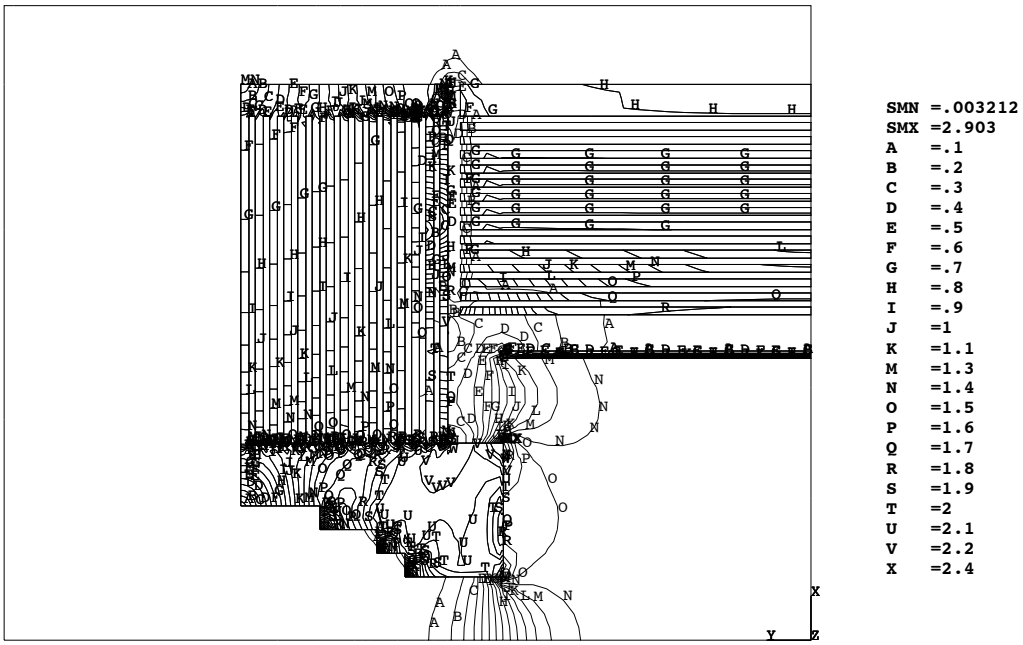

(a) Magnetic-field contour map

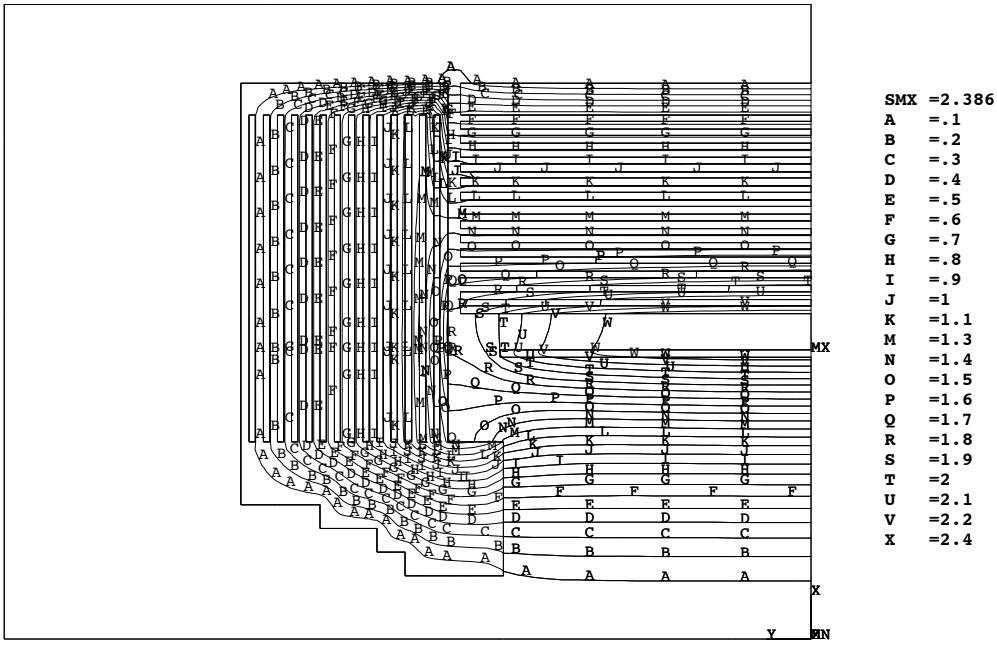

(b) Magnetic flux line display

Figure 8.13: Contour map and flux line display of the magnetic field.

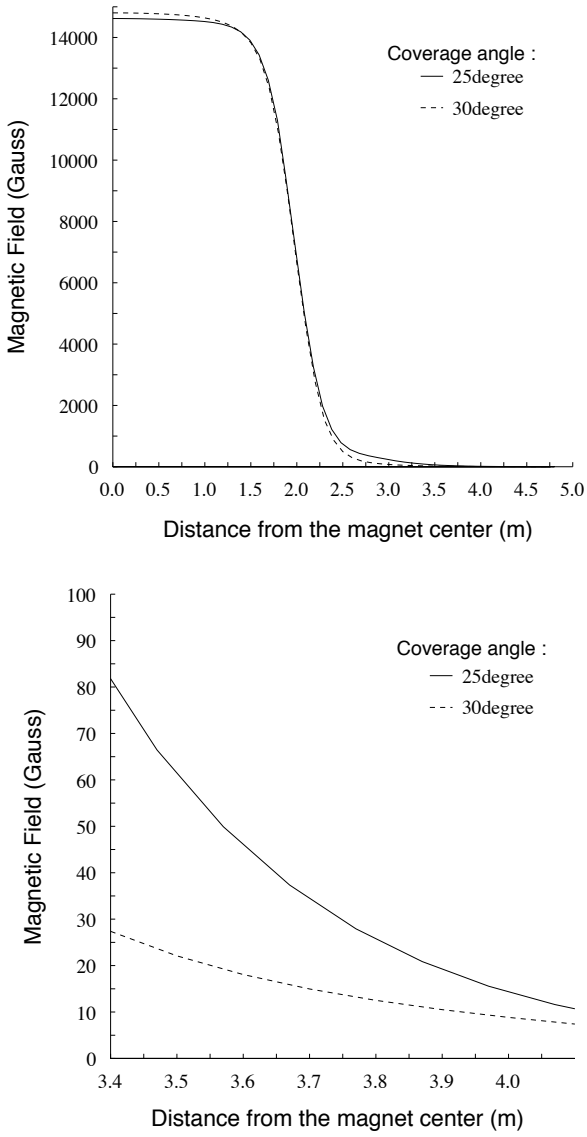

Figure 8.14: The magnetic field along the beam axis.

Bibliography

[1] Y. Makida *et al.* , "Performance of a thin superconducting solenoid for particle astrophysics", Adv.Cryog.Eng., **37**, p401 (1992).